Preprints of the 19th World Congress
The International Federation of Automatic Control
Cape Town, South Africa. August 24-29, 2014

Modeling and μ-synthesis Based Robust Trajectory Tracking Control of a Wheeled Mobile Robot

Zheyu Deng * **Bin Yao** *,** **Xiaocong Zhu** * **Qingfeng Wang** *
Huayong Yang *

* *The State Key Laboratory of Fluid Power Transmission and Control, Zhejiang University, Hangzhou, 310027, China (e-mails: dengzy, byao, zhuxiaoc, qfwang@zju.edu.cn).*
** *School of Mechanical Engineering, Purdue University, West Lafayette, IN47907, USA.*

Abstract: Performance of trajectory tracking is important for Wheeled Mobile Robots (WMR), which have wide applications in industry, medical treatment, and domestic service, etc. In this paper, comprehensive modeling of a WMR is presented with model parameters estimated via system identification. The influence on experimental frequency response due to friction disturbances at low frequency and modeling uncertainties at high frequency are carefully analyzed. To achieve higher trajectory-tracking performance, both the non-holonomic kinematic constraints and the dynamics of actual WMRs are taken into account, and a -synthesis based robust control method is presented to deal with the friction disturbances and the high-frequency modeling errors. Comparative experimental results are also obtained to verify the effectiveness of the proposed control strategy in actual implementation.

Keywords: μ-synthesis control; non-holonomic constraints; modeling; trajectory tracking; wheeled mobile robot

1. INTRODUCTION

Wheeled mobile robots (WMR) are used in many applications due to its ability of handling complex visual and information processing for artificial intelligence and the simplicity and high energy efficiency of its engineering design. There have been quite a lot of research done on the motion control of WMR. Due to the non-holonomic constraints inherited in WMR (Campion et al. (1996)), both the kinematic and dynamic models of WMR need to be taken into account when synthesizing a controller, in addition to the stable motion planning at the kinematic level in (Kanayama et al. (1990)).

In terms of trajectory tracking control of WMRs, there have been many methods proposed for high speed and high tracking accuracy. In industry, the PID feedback control method is widely used due to its simplicity for implementation. However, it is difficult to achieve high precision tracking control performance for the complicated WMR system with the simple PID method. For example, in our experiment kit shown in Fig. 1, relative large disturbances and model uncertainties exist in a certain range of frequency domain. As will be seen later, it is insufficient to use the simple PID control method

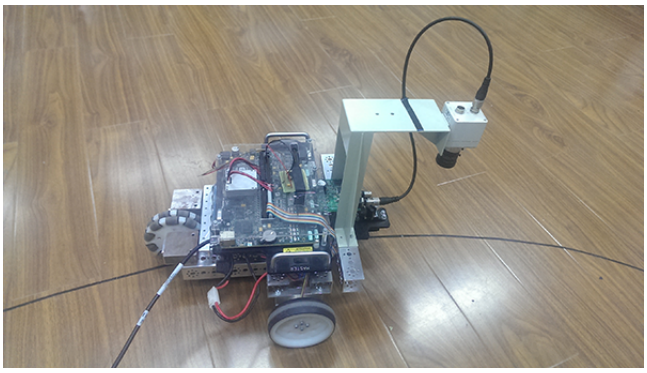

Fig. 1. Wheeled mobile robot with CCD camera

to attenuate the effect of those external disturbances and model uncertainties. Fuzzy control method has been used for WRM systems in unstructured environments (Watanabe et al. (1996); Saffiotti et al. (1999)). However, the design of system functions is mostly based on personal experience and the fuzzy control lacks of systematic ways to make full use of the known structure of the dynamic models of WMR. Adaptive control laws have also been proposed (Mohareri et al. (2012); Klancar and Skrjanc (2007); Shojaei et al. (2011); Yeh et al. (2009); Kunhe et al. (2005)). These algorithms are mainly to deal with the issue of unknown parameters in the dynamics of WMR without clearly addressing the effect of external disturbances and other modeling uncertainties. Hwang used H_2/H_∞ control method to attenuate the effect of output disturbances (Hwang and Han (2005); Hwang and Chang (2007)), but

⋆ This work is supported in part by the Fundamental Research Funds for the Central Universities (2013QNA4006), the National Basic Research and Development Program of China under 973 Program Grant 2013CB035400, and the Science Fund for Creative Research Groups of National Natural Science Foundation of China (No: 51221004).

without addressing the effect of other model uncertainties. Solea and Park applied sliding mode control methods to the control of WMR systems with matched model uncertainties and external disturbances only (Solea et al. (2010); Park et al. (2009)).

In this paper, complete kinematic and dynamic models of a WMR will be presented, with the model parameters estimated through identification experiments. The effect of disturbances in the low frequency and the modeling uncertainty in high frequency will be carefully examined with the frequency response experiments. To achieve a higher trajectory tracking performance of the WMR, a control strategy having inner and outer loops is used. In the outer loop, the stable trajectory tracking control rule at the kinematic level proposed by Kanayama in (Kanayama et al. (1990)) will be utilized to deal with the non-holonomic constraints in WMR and implemented with a relatively larger sampling period. In the inner loop, a μ-synthesis (Balas et al. (2005)) based robust control algorithm will be developed to deal with the friction disturbances and modeling uncertainties in high-frequency dynamics and implemented with a relatively smaller sampling period. Comparative experimental results will be presented to verify the effectiveness of the proposed control strategy in actual implementation.

2. SYSTEM DESCRIPTION

Fig. 1 shows the prototype of the wheeled mobile robot with a CCD camera for experiments. The main body is a NI Labview Robotics Starter Kit 2.0 with a NI Single-Board 9632 and Labview programming language. Within the graphic programming language Labveiw hardware environment, there are two main parts: real-time module and FPGA module. Complicated mathematical calculations are signal processing are always carried out in the real-time module while the FPGA module is mainly used to communicate data with sensors and actuators. Some simple mathematical algorithms can also be run in FPGA to achieve a relative high processing speed. In the Robotics Starter Kit 2.0, NI corporation has embedded a dual DC motor driver, two DC motors, two digital Encoders to FPGA in Single-Board 9632. The dual DC motor driver is Sabertooth 2*10 R/C with voltage output to control two DC motors at the same time. The motors specifications are : supply voltage 12V, empty load speed 146 RPM, empty load current 0.17 Amps, torque 300 oz-in. The encoders specifications are: supply voltage 5V, cycles per revolution 100CPR, pulses per revolution 400 CPR, which leads to an angular measurement resolution of 0.9°. A CCD camera is also placed in the front of Robotics Starter Kit 2.0 with its image information sent to PFGA in Single-Board 9632 though frame grabber. As the encoders' resolution is not high enough, an inertial sensor ADIS16375 is added to measure the angular velocity of the robot car, which has an angular velocity measurement resolution of $0.013108°/s$.

2.1 Dynamic model of WMR

The schematic diagram of the WMR and the associated coordinate systems are shown below Consider the situation that the WMR is on a level surface so that the gravity effect is ignored for simplicity. Let $[x_o, y_o]$ be the coordinates

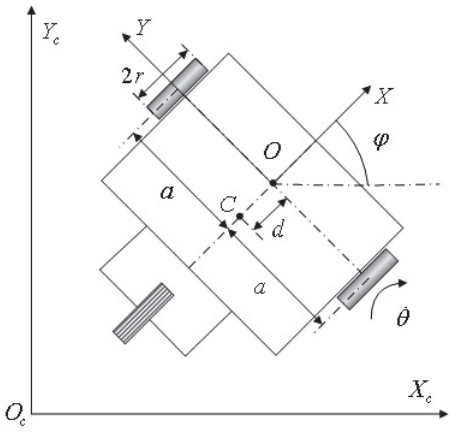

Fig. 2. Mobile robot with non-holonomic constraints

of the point O in the world frame and φ be the rotational angle of the WMR. Under the assumption that there is no slip between tires and the ground, the dynamic model of the WMR body can be obtain through Lagrange equation as

$$M(q)\ddot{q} + V_m(q,\dot{q})\dot{q} + F(\dot{q}) + \tau_d = B(q)\tau - A^T(q)\lambda \quad (1)$$

where $q = (x_o, y_o, \varphi)$ represent the generalized coordinates of the WMR, in which $M(q)$ is the symmetric positive definite inertia matrix, $V_m(q,\dot{q})$ is the centripetal and coriolis matrix, $F(\dot{q})$ is the surface friction vector, τ_d denotes the vector unknown disturbances including unmodeled forces, $B(q)$ is the input transformation matrix, τ is the drive forces vector, $A(q) = [\sin\varphi, \cos\varphi, 0]$ is the matrix associated with the non-holonomic constrains given by

$$A(q)\dot{q} = 0 \quad (2)$$

and λ is the constraint forces vector.

Let $S(q)$ be a full rank matrix (n-m) formed by a set of smooth and linearly independent vector fields spanning the null space of $A(q)$ as (Sarkar et al. (1994))

$$A(q)S(q) = [\,-\sin\varphi \;\; \cos\varphi \;\; 0\,] \begin{bmatrix} \cos\varphi & 0 \\ \sin\varphi & 0 \\ 0 & 1 \end{bmatrix} = 0 \quad (3)$$

The derivatives of the generalized coordinates are then related to the velocity vector of the WMR as

$$\dot{q} = \begin{bmatrix} \cos\varphi & 0 \\ \sin\varphi & 0 \\ 0 & 1 \end{bmatrix} \begin{bmatrix} v \\ w \end{bmatrix} = S(q)v(t) \quad (4)$$

where v is the froward speed and w is the angular velocity. Substituting (2), (3) and (4) into (1) and removing the unknown constraint force vector λ, the following motion equations are obtained (Mohareri et al. (2012))

$$\begin{bmatrix} m & 0 \\ 0 & I \end{bmatrix} \begin{bmatrix} \dot{v} \\ \dot{w} \end{bmatrix} - \begin{bmatrix} 0 & mdw \\ -mdw & 0 \end{bmatrix} \begin{bmatrix} v \\ w \end{bmatrix} = P^T \begin{bmatrix} \tau_1 \\ \tau_2 \end{bmatrix} + \begin{bmatrix} F_d \\ \tau_d \end{bmatrix}, \quad P = \begin{bmatrix} 1/r & a/r \\ 1/r & -a/r \end{bmatrix} \quad (5)$$

where m is the mass of WMR, I is the rotational inertia around the point O, r is the radius of two drive wheels, a is the half distance between the two drive wheels, τ_1 and τ_2 are the left and right drive torques that come form

the friction between wheels and the ground, F_d and τ_d are disturbance force and torque come from $F(\dot{q})$ and τ_d vectors. The drive torques from frictions are related to the output torques of the motors by

$$\begin{bmatrix} \tau_1 \\ \tau_2 \end{bmatrix} = \begin{bmatrix} \tau_r \\ \tau_l \end{bmatrix} - J_w P \begin{bmatrix} \dot{v} \\ \dot{w} \end{bmatrix} - b_w P \begin{bmatrix} v \\ w \end{bmatrix} \tag{6}$$

where τ_r and τ_l are the output torques of the two motors, J_w is the rotational inertia of the drive wheels, b_w is the viscous damping coefficient in the motor shaft. The electromechanical model of the DC motor is

$$\begin{bmatrix} U_r \\ U_l \end{bmatrix} - K_e P \begin{bmatrix} v \\ w \end{bmatrix} = \frac{L}{K_i} \begin{bmatrix} \dot{\tau}_r \\ \dot{\tau}_l \end{bmatrix} + \frac{R}{K_i} \begin{bmatrix} \tau_r \\ \tau_l \end{bmatrix} \tag{7}$$

where U_r and U_l are the input voltages to the motors, K_e is the back electromotive force constant, K_i is the torque constant, L is the equivalent inductance, and R is the equivalent resistance of the motor. Combining (5), (6), (7), the dynamic model of the WMR system is obtained as

$$X_{\ddot{V}}\ddot{V} + X_{\dot{V}}\dot{V} + X_V V = U - D \tag{8}$$

where

$$\begin{aligned}
&V = \begin{bmatrix} v \\ w \end{bmatrix},\ U = \begin{bmatrix} U_r \\ U_l \end{bmatrix},\ D = \begin{bmatrix} F_d \\ \tau_d \end{bmatrix} \\
&X_V = \begin{bmatrix} \beta_1 + \beta_2 + \beta_3 w + \beta_4 \dot{w} & a(\beta_1 + \beta_2 - \beta_3 w - \beta_4 \dot{w}) \\ \beta_1 + \beta_2 - \beta_3 w - \beta_4 \dot{w} & a(-\beta_1 - \beta_2 - \beta_3 w - \beta_4 \dot{w}) \end{bmatrix} \\
&X_{\dot{V}} = \begin{bmatrix} \beta_5 + \beta_6 w + \beta_7 + \beta_8 & a(\beta_5 - \beta_6 w + \beta_8) + \beta_9 \\ \beta_5 - \beta_6 w + \beta_7 + \beta_8 & -a(\beta_5 - \beta_6 w - \beta_8) - \beta_9 \end{bmatrix} \\
&X_{\ddot{V}} = \begin{bmatrix} \beta_{10} + \beta_{11} & a\beta_{10} + \beta_{12} \\ \beta_{10} + \beta_{11} & -a\beta_{10} + \beta_{12} \end{bmatrix} \\
&\beta_1 = \frac{K_e}{r}, \beta_2 = \frac{Rb_w}{rK_i}, \beta_3 = \frac{Rdmr}{2aK_i}, \beta_4 = \frac{Ldmr}{2aK_i} \\
&\beta_5 = \frac{Lb_w}{rK_i}, \beta_6 = \frac{Ldmr}{2aK_i}, \beta_7 = \frac{Rmr}{2K_i}, \beta_8 = \frac{J_w R}{rK_i} \\
&\beta_9 = \frac{RIr}{2aK_i}, \beta_{10} = \frac{J_w L}{rK_i}, \beta_{11} = \frac{Lmr}{2K_i}, \beta_{12} = \frac{LIr}{2aK_i}
\end{aligned} \tag{9}$$

2.2 Model simplification and problem formulation

For the WMD under study, the coupling terms β_3,β_4 and β_6 are 3 orders of magnitude smaller than other terms and the actual angular velocity w is less than 5 rad/s. In addition, the coupling terms have negligible effect on the system dynamics and can also be neglected. With these simplifications, the following model of WMR is obtained after ignoring the disturbances for time being:

$$\begin{bmatrix} v \\ w \end{bmatrix} = G(s) \begin{bmatrix} u_1 \\ u_2 \end{bmatrix} = \begin{bmatrix} \dfrac{41.6667}{(s+95.1011)(s+10.7318)} & 0 \\ 0 & \dfrac{341.9973}{(s+88.8735)(s+16.8725)} \end{bmatrix} \begin{bmatrix} u_1 \\ u_2 \end{bmatrix} \tag{10}$$

Furthermore, as shown in Fig 3, the following pre-compensation matrix can be added to decouple the $G(s)$ matrix:

$$C_{pre} = \begin{bmatrix} 0.5 & 0.5 \\ 0.5 & -0.5 \end{bmatrix} \tag{11}$$

which leads to the following decoupled transfer function matrix:

$$\bar{G}(s) = G(s)C_{pre} = \begin{bmatrix} \dfrac{41.6667}{(s+95.1011)(s+10.7318)} & 0 \\ 0 & \dfrac{341.9973}{(s+88.8735)(s+16.8725)} \end{bmatrix} \tag{12}$$

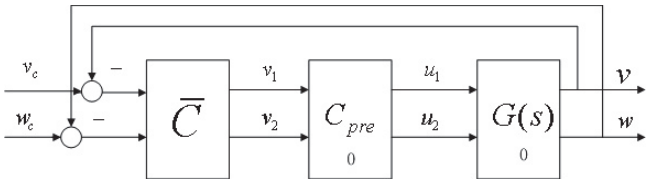

Fig. 3. Pre-compensator in control design

Frequency response experiments are then carried out to verify the correctness of this simplified model and to investigate the effect of the neglected disturbances and model uncertainties. For the experimental WMR system, the forward velocity of the robot car is calculated from the encoders' reading, which does not a high enough accuracy due to the resolution of encoders. Due to this hardware constraints, the control of the forward velocity will not be considered in this paper and only the control of the angular velocity is studied, which also has a much more significant effect on the performance of WMR's trajectory-tracking. In the frequency response experiments, the input

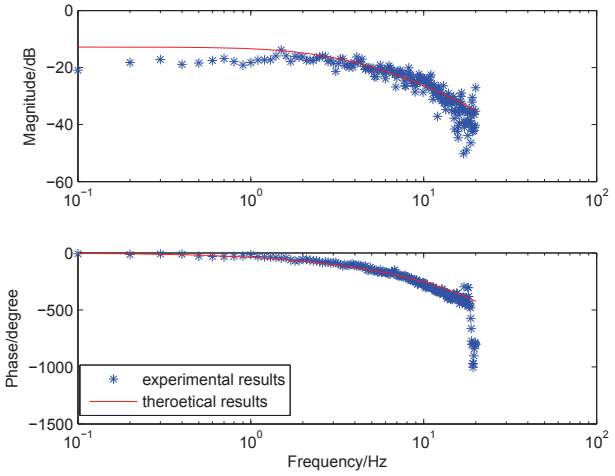

Fig. 4. Frequency responses of angular velocity

voltage signal is chosen to be a sum of sinusoidal signals ranging from 0.1Hz to 20Hz, with a frequency interval of 0.1Hz and magnitude of 10V. The obtained frequency responses of the angular velocity are shown in Fig. 4. As seen from the figure, the phase plots of the experimental frequency response and that predicted by the model in (12) are almost same, but there are some differences in the magnitude plots. Specifically, in the low frequency from 0.1Hz to 1Hz, the magnitude plot of the experimental frequency response is almost flat but below the value predicted by the theoretical model in (12), indicating that significant disturbances in the low frequency domain mainly due to the friction effect. In the relatively higher frequency range from 5Hz to 20Hz, though the magnitude plots of the two frequency responses are correlated with each other well, the experimental frequency response has very significant fluctuations, indicating that some model

uncertainties may exist. The model uncertainties may be caused by the flexibility of the camera support frame and other mechanical parts; as the WMR moves, the camera support frame shakes slightly.

3. CONTROL SYSTEM DESIGN

3.1 Controller structure

As the image data processing needs a time of 200ms, a two-loop controller structure is used, as shown in Fig. 5. In the outer loop, the real-time WMR's position and posture information are obtained through analyzing the image information in Labview, from which the reference velocities of the WMR for the inner-loop design are calculated with the stable tracking control rule in (Kanayama et al. (1990)) as

$$\begin{pmatrix} v_c \\ w_c \end{pmatrix} = \begin{pmatrix} v_r \cos\theta_e + K_x y_e \\ w_r + v_r(K_y x_e + K_\theta \sin\theta_e) \end{pmatrix} \tag{13}$$

where v_r and w_r are the reference forward and angular velocities, $\{x_e, y_e, \theta_e\}$ is the posture error vector which is the discrepancy between the reference posture and current posture, K_x, K_y and K_θ are positive constants. In the inner loop, the forward velocity and angular velocity controllers run in the Labview PFGA module with a smaller sampling period of 20ms so that the Nyquist frequency of the velocity controller loop can reach 25Hz for better dynamic responses and disturbance rejections.

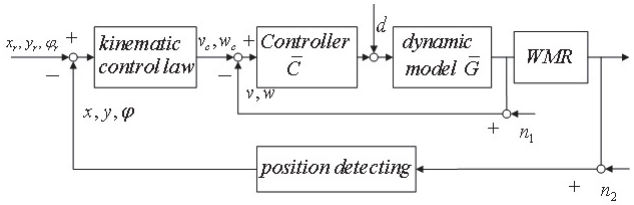

Fig. 5. Controller structure

3.2 μ-synthesis based robust controller design

H_∞ robust control theory has been well-documented in literature (e.g., Zhou and Doyle (1998)) and it is very convenient to design a μ-controller using robust control toolbox in MATLAB. So it will be used to synthesize the inner-loop controllers in this subsection. In principle, H_∞ robust control theory is concerned with finding a controller $K(s)$ that minimizes the H_∞ norm of the transfer function matrix T_{zw} from the external inputs w and to the outputs z. By minimizing the peak value or improving the worst-case scenario, it renders magnitude of T_{zw} small at all frequencies. Usually a controller $K(s)$ can be solved to guarantee a bound $\|T_{zw}\|_\infty < \gamma$. By the small gain theorem, such a guaranteed bound can also guarantee the stability of the closed-loop systems with uncertainties satisfying $\|\Delta\|_\infty < \frac{1}{\gamma}$, i.e., the robust stability of the closed loop system is achieved (Zames (1966)). In applying H_∞ robust control theory, it is critical to choose appropriate weighting functions to account for the relative magnitudes, frequency dependence, and relative importance of various input and output signals. As such selection of weighting functions is explained in details as follows. With the

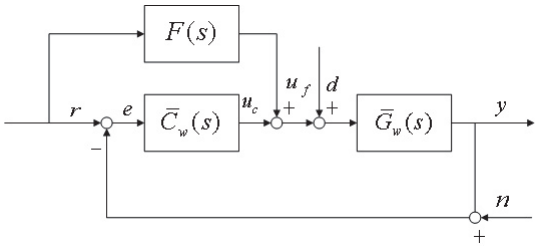

Fig. 6. Inner-loop controller structure

inner-loop controller structure shown in Fig 6 and the feedforward transfer function matrix $F(s)$ synthesized such that $\bar{G}_w(s)F(s) \approx I$,

$$y = \bar{G}_w(u+d) = \bar{G}_w[\bar{C}_w(s)(r-y-n)+d] \tag{14}$$

Letting $e = r - y$, then

$$-e = \bar{G}_w[\bar{C}_w(s)(e-n)+d] + d_o \tag{15}$$

where $d_o = [\bar{G}_w(s)F(s) - 1]r$ represents the feedforward model compensation error. By doing so, the problem of velocity tracking control is transformed into a stabilization problem shown in Fig. 7 that is easier to choose the weighting functions, in which the model compensation error d_o is treated as the output disturbance. A general principle in choosing the weighting functions is that a larger value of weighting should be used if the related signal is more important.

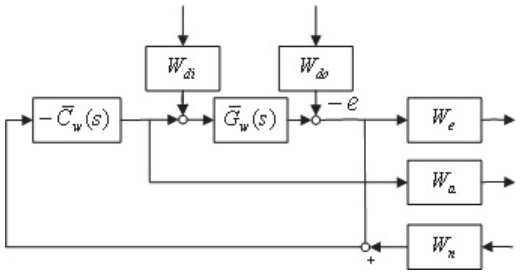

Fig. 7. H_∞ synthesis with weighting functions

Usually W_n is derived from laboratory experiments or based on manufacturer specifications. As the angular velocity noise signals measured by ADIS 16375 is about 0.02 rad/s, W_n is chosen to be a constant value of 0.02

$$W_n = 0.02 \tag{16}$$

W_{di} shapes the frequency content and magnitude of the exogenous disturbances effecting the plant. Since significant disturbances exist in low frequency especially at frequency less than 1Hz, W_{di} is chosen to have a relative high value 1000 at low frequency and drop fast over a finite frequency range; a higher bandwidth of W_{di} normally leads to a synthesized close-loop system of higher bandwidth, which may not be achievable in reality. With these consideration, a second-order transfer function of W_{di} is chosen:

$$W_{di} = \frac{10}{s^2 + 0.8s + 0.01} \tag{17}$$

As the output disturbance d_o is supposed to be negligible due to the use of feedforward compensation, W_{do} is set as 0 for simplicity. For W_e, the weighting function is chosen

to be a large constant value to reflect the design emphasis of smaller tracking error:

$$W_e = 80 \tag{18}$$

W_a is used to shape the penalty on control input. As our targeted frequency range is up to 25Hz and the control input saturation is not a significant problem, W_a is simply chosen to be a constant value 1. A parametrized uncer-

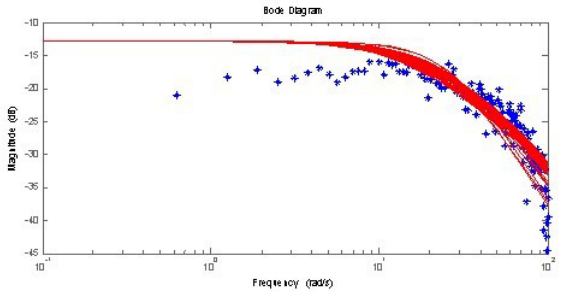

Fig. 8. Frequency response of dynamic model with uncertainty

tainty model is also used to cover the model uncertainties exiting in the high frequency range of 5Hz to 20Hz, as shown in Fig.8. The uncertainty model has two uncertain parameters. Parameter 1 has a range of [0.0005968, 0.001968] and parameter 2 has a range of [0.0656, 0.0856], as shown in (20).

$$\bar{G}_w(s) = \frac{0.2287}{para1 \cdot s^2 + para2 \cdot s + 1} \tag{19}$$

With the above weight functions and the uncertainty model, μ-synthesis approach is used to synthesized a controller to ensure a guaranteed robust stability and disturbance rejection performance for stated uncertainties. The bode diagrams of the transfer functions from the noise to the error, the input disturbance to the error, the output disturbance to the error and the control input to the error are shown in Fig. 9.

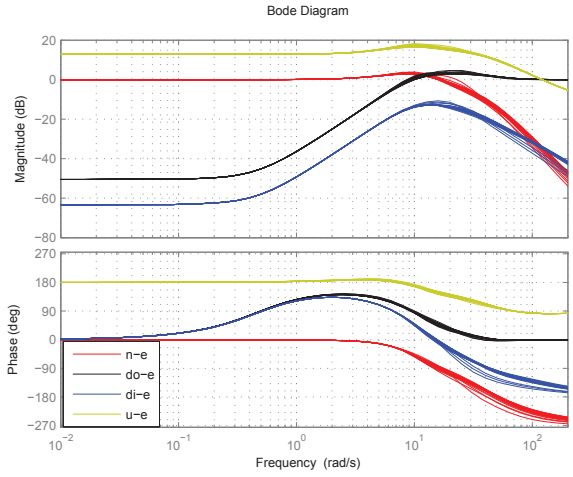

Fig. 9. Board diagram of the closed-loop system

The details of the robustness analysis are:

1)Stability

- Uncertain System is robustly stable to modeled uncertainty.

-It can tolerate up to 108% of the modeled uncertainty.

-A destabilizing combination of 111% of the modeled uncertainty exists, causing an instability at 0.341 rad/s.

-Sensitivity with respect to uncertain element. 'parameter1' is 124% . Increasing 'parameter1' by 25% leads to a 31% decrease in the margin. 'paremeter2' is 21%. Increasing 'paremeter2' by 25% leads to a 5% decrease in the margin.

2)Performance

-Uncertain System achieves a robust performance margin of 0.001002.

-A model uncertainty exists of size 0.1% resulting in a performance margin of 998 at 2.54e-005 rad/sec.

-Sensitivity with respect to uncertain element. 'parameter1' is 0%. Increasing 'parameter1' by 25% leads to a 0% decrease in the margin. 'paremeter2' is 0%. Increasing 'parameter2' by 25% leads to a 0% decrease in the margin.

4. EXPERIMENTAL RESULTS

4.1 Experiment setup

Experiments are carried out on the the robot car in Fig. 1 to examine the effectiveness of the proposed controller. For comparison, a standard PID controller instead of the proposed μ-synthesis based controller is also implemented in the inner-loop in Fig.6.

4.2 Performance Indexes

To measure the quality of each control algorithm, the following performance indexes will be used :

$e_M = \max_t\{|e|\}$, the maximum absolute value of the tracking error is used to measure transient performance;

$e_F = \max_{T-10\le t\le T}\{|e|\}$, the maximum absolute value of the tracking error during the last 10 seconds, is used as an index of measure of final tracking accuracy;

$\|e\|_{rms} = (\frac{1}{T}\int_0^T |e|^2 dt)^{1/2}$, the RMS value of the tracking error, is used to measure average tracking performance.

4.3 Comparative Experimental result

In the first set of experiments, a sinusoidal velocity command of magnitude of 2 rad/s and frequency of 0.2 Hz is directly given to the angular velocity loop to test the tracking performance of the PID controller and the proposed μ-synthesis controller. The results are shown in Fig. 10 and Table 1. As the motors have a relatively large dead

Table 1. Experimental results

indexes	$e_M(rad/s)$	$e_F(rad/s)$	$\|e\|_{rms}(rad/s)$
PID	0.4545	0.2515	0.1198
μ-synthesis	0.5298	0.1153	0.0610

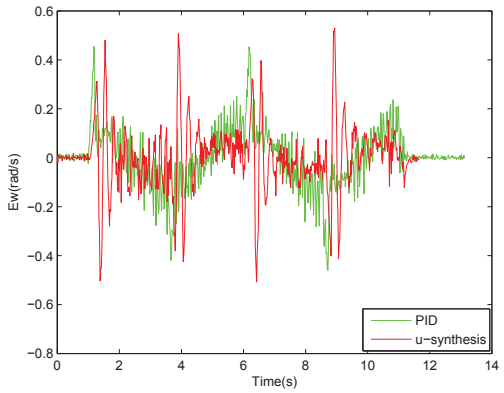

Fig. 10. Velocity tracking errors

zone when the rotational speeds cross zero, the transient performance indexes are almost the same for the two controllers. However, μ-synthesis achieves a better average tracking performance and a smaller maximum tracking error during the last 10 seconds, as seen from the values of $\|e\|_{rms}$ and e_F for two controllers. This indicates that the proposed μ-synthesis controller has a better disturbance rejection and robust performance.

In the second set of experiments, the WMR is commanded to track an elliptic trajectory and the two-loop controller structure shown in Fig.5 with the velocity command for the inner-loop generated by (13). The elliptic trajectory has a long axis of 2.26m and a short axis of 1.6m. As the width of the picture that the CCD camera can catch is 0.13m, the robot cannot track the trajectory when the Y position error is more than 0.0675m or half of 0.13m. In the experiments, when the reference forward velocity is set at 0.4 m/s, the WMR cannot track the elliptic trajectory at the large curvature part of the ellipse when the PID controller is used in the angular velocity loop. However, the WMR can still track the same elliptic trajectory when the proposed μ-synthesis controller is used, indicating the better tracking performance of the proposed controller.

5. CONCLUSION

In this paper, complete kinematic and dynamic models of a WMR have been obtained with the model parameters estimated through identification experiments. A control strategy having inner and outer loops has been developed to obtain better trajectory tracking performance. Specifically, motion planning for stable trajectory tracking was carried out in the outer loop to address the nonholonomic kinematic constraints inherited in WMR. It is implemented with a relatively larger sampling period to address the potential heavy computation needs of real-time motion planning with visual feedback. A μ-synthesis based robust control algorithm was used in the inner loop and implemented at a higher sampling rate to achieve better disturbance attenuation and robust control performance in the presence of modeling uncertainties. Comparative experimental results have been obtained to verify the effectiveness of the proposed control strategy in actual implementation.

REFERENCES

Balas, G., Chiang, R., Packard, A., and Safonov, M. (2005). Robust control toolbox users guide, version 3.

Campion, G., Bastin, G., and Dandrea-Novel, B. (1996). Structural properties and classification of kinematic and dynamic models of wheeled mobile robots. *IEEE Transactions on Robotics and Automation*, 12(1), 47–62.

Hansen, L.P. and Sargent, T.J. (2001). Robust control and model uncertainty. *The American Economic Review*, 91(2), 60–66.

Hwang, C.L. and Chang, L.J. (2007). Trajectory tracking and obstacle avoidance of car-like mobile robots in an intelligent space using mixed H_2/H_∞ decentralized control. *IEEE/ASME Transactions on Mechatronics*, 12(3), 345–352.

Hwang, C.L. and Han, S.Y. (2005). Mixed H_2/H_∞ design for a decentralized discrete variable structure control with application to mobile robots. *IEEE Transactions on Systems, Man, and Cybernetics, Part B: Cybernetics*, 35(4), 736–750.

Kanayama, Y., Kimura, Y., Miyazaki, F., and Noguchi, T. (1990). A stable tracking control method for an autonomous mobile robot. In *Proceedings of IEEE International Conference on Robotics and Automation* , 384–389.

Klancar, G. and Skrjanc, I. (2007). Tracking-error model-based predictive control for mobile robots in real time. *Robotics and Autonomous Systems*, 55(6), 460–469.

Kunhe, F., Gomes, J., and Fetter, W. (2005). Mobile robot trajectory tracking using model predictive control. *II IEEE Latin-american Robotics Symposium*.

McDonald, K.A., Palazoglu, A., and Bequette, B.W. (1988). Impact of model uncertainty descriptions for high-purity distillation control. *AIChE journal*, 34(12), 1996–2004.

Mohareri, O., Dhaouadi, R., and Rad, A.B. (2012). Indirect adaptive tracking control of a nonholonomic mobile robot via neural networks. *Neurocomputing*, 88, 54–66.

Park, B.S., Yoo, S.J., Park, J.B., and Choi, Y.H. (2009). Adaptive neural sliding mode control of nonholonomic wheeled mobile robots with model uncertainty. *IEEE Transactions on Control Systems Technology*, 17(1), 207–214.

Saffiotti, A., Ruspini, E.H., and Konolige, K. (1999). Using fuzzy logic for mobile robot control. in *Practical applications of fuzzy technologies*, 185–205. Springer.

Sarkar, N., Yun, X., and Kumar, V. (1994). Control of mechanical systems with rolling constraints application to dynamic control of mobile robots. *The International Journal of Robotics Research*, 13(1), 55–69.

Shojaei, K., Shahri, A.M., Tarakameh, A., and Tabibian, B. (2011). Adaptive trajectory tracking control of a differential drive wheeled mobile robot. *Robotica*, 29(3), 391–402.

Solea, R., Filipescu, A., Minzu, V., and Filipescu, S. (2010). Sliding-mode trajectory-tracking control for a four-wheel-steering vehicle. In *8th IEEE International Conference on Control and Automation (ICCA)*, 382–387.

Tian, Y., Sidek, N., and Sarkar, N. (2009). Modeling and control of a nonholonomic wheeled mobile robot with wheel slip dynamics. In *IEEE Symposium on Computational Intelligence in Control and Automation*, 7–14.

Watanabe, K., Tang, J., Nakamura, M., Koga, S., and Fukuda, T. (1996). A fuzzy-gaussian neural network and its application to mobile robot control. *IEEE Transactions on Control Systems Technology*, 4(2), 193–199.

Yeh, Y.C., Li, T.H.S., and Chen, C.Y. (2009). Adaptive fuzzy sliding-mode control of dynamic model based car-like mobile robot. *International Journal of Fuzzy Systems*, 11(4), 272–286.

Zames, G. (1966). On the input-output stability of time-varying nonlinear feedback systems part one: Conditions derived using concepts of loop gain, conicity, and positivity. *IEEE Transactions on Automatic Control*, 11(2), 228–238.

Zhou, K. and Doyle, J.C. (1998). *Essentials of robust control*, Prentice Hall, Upper Saddle River, NJ.